J. Acoust. Soc. Jpn. (*E*) **18**, 2 (1997)

Acoustic streaming by ultrasonic vibrating electrode (USVE)

Nobuhide Tatsumoto, Nagamasa Kawano, and Shigetada Fujii

General Education Chemistry and Physics, Faculty of Medicine, Oita Medical University, 1-1, Idaigaoka, Hasama-machi, Oita, 879-55 Japan

(*Received 22 February 1996*)

In a voltammetry employing an electrode with a diameter of 2 mm, vibrating at ultrasonic frequecy of 38 kHz and at an amplitude of 0.5 through 3 μm_{p-p}, acoustic streamings were investigated by the flow visualizing experiment and the analysis of a two-dimensional finite element method. The experiment revealed that a gas bubble was generated on the electrode surface at the amplitude above 0.7 μm_{p-p}, and the vibrating mode of the bubble played an important role in the acoustic streaming. These mechanisms were successfully simulated by the analysis assuming a vortex pair located on the electrode.

Keywords: Acoustic streaming, Ultrasonic vibrating electrode, Voltammetry

PACS number: 43. 25. Nm, 43. 25. Ym

1. INTRODUCTION

High sensitive chemical analysis can be performed with the voltammetry by measuring the electric voltage and current in electrolyte solution. The residual electric current subtracted the current by supporting solvent from the total current is stationary during the oxidation or the reduction reaction and it is proportional to the concentration of the solute. Then the small amount of solute can be detected by voltammetry. In the early stage of this method, stationary solid electrodes were used. To take more precise measurements, external forcing flow methods such as hydrodynamic modulation voltammetry,[1-5] pulse-rotation voltammetry,[6] the stopped-flow technique[7] and rotating disc electrode voltammetry, have been widely used. On the other hand, methods applying ultrasonic irradiation to the solid electrode surface or vibrating wire electrode technique[8-13] have been reported. We have reported a new voltammetry using an ultrasonic vibrating electrode in which the sensitivity was considerably enhanced in the oxidization reaction of chlorpromazine as a test sample.[14] However, measurements or detailed analysis of the flow fields by the above methods have not been performed. If reaction products accumulate near the electrode surface, exchange reaction with unreacted substance will be extremely hindered, which will lead to the lowered sensitivity of the analysis.

In this study, we have tried to clarify the detailed flow profile of solution by a visual observation and a numerical simulation in the ultrasonically vibrating electrode voltammetry. These results will help to know the conditions of the effective exchange between reactant and reaction products created by acoustic flow of solution. Thus an optimum condition of the measurements will be obtained.

While most of the studies on the acoustic streaming have been done at a high vibrating frequency and a high output power, the ultrasonic source in our voltammetry employed the frequency of 38 kHz, and the input electrical power to an oscillator electrode of 2 mm diameter was only about 10 W. Thus the velocity of the acoustic streaming was estimated to be at most a few cm/s. Detailed studies on such a low power acoustic streaming have not been done so far. The experiment of the present method of voltammetry revealed that the measured values of the electric current were extremely unstable and less reproducible about at both the vibrational displacements of about 0.7 μm_{p-p} and 1.8 μm_{p-p}. The former might be due to the generation and growth of a gas bubble due to cavitation on the electrode surface, and the latter might be due to the change in the vibrating mode of the bubble. S. A. Edler[15] has reported that the gas bubble due to cavitation is generated when a ultrasonic wave is irradiated vertically to the flat wall and then a vibrating cavitation microstreaming occurs. In this study the authors conducted the flow visualization experiment and the numerical simulation in which a 2-dimensional finite element method was used for investigating the acoustic streaming.

2. FLOW VISUALIZING EXPERIMENT

The solution of K_2SO_4 (0.1 mol/l) suspending a small amount of alumina particles ($<$1 mmϕ) as flow tracers was placed in a rectangular vessel whose inside width, depth and height were 40 mm, 40 mm and 70 mm respecitively, as shown in Fig. 1. The flow field on a plane containing the electrode was illuminated by a xenon lamp through a slit of 1 mm width, and the path lines of the flow were recorded by a video camera and a still camera. It should be especially noted that the acoustic streaming was hardly observed below the electrode's vibrating amplitude of 0.5 μm_{p-p}, but above 0.7 μm_{p-p} a gas bubble appeared irregularly on the electrode surface, and it disappeared after expansion, and at the same time the downward streaming was ejected perpendicularly from the electrode surface. Such a behaviour seems to make the flow neither stable nor stationary. With the increase of the vibrating amplitude in the range of 0.8–1.6 μm_{p-p}, a gas bubble with a diameter upto 0.2 mm appeared and vibrated continuously and steadily. The concomitantly performed straight downward flow was stable and seemed to make the solution exchange effective. At the amplitude of 1.8 μm_{p-p} the electric current in the voltammetry became unstable but the gas bubble remained like a oblate sphere and seemed to take a strong downward pumping action where its changing position and shape could hardly be discriminat-

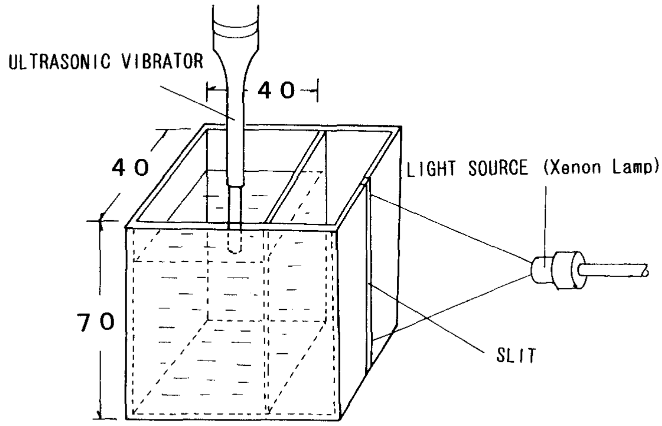

Fig. 1 Vessel for flow visualizing use.

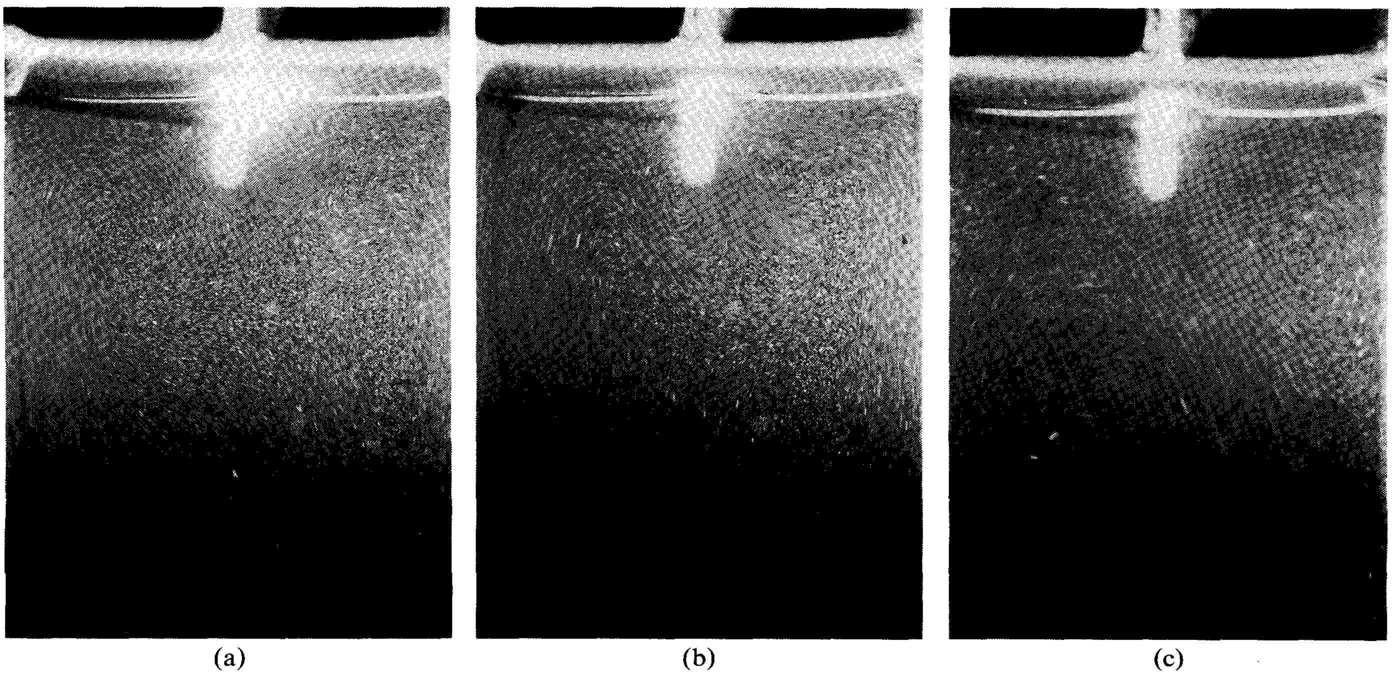

Fig. 2 (a) Photograph of flow path lines at electrode amplitude 1.5 μm_{p-p}. (b) Flow path lines at electrode amplitude 2 μm_{p-p}. (c) Flow path lines at electrode amplitude 3 μm_{p-p}.

ed. Therefore it is plausible to condsider that the strong pumping action is due to the shift of another vibrating mode. In Figs. 2(a), 2(b) and 2(c), the path lines in the flows at the amplitudes of 1.5, 2, 3 μm_{p-p} are shown respectively. The maximum speed of flows is $1\text{-}3\times 10^{-2}$ m/s judging by a data reduction from video pictures.

3. NUMERICAL SIMULATION

There are several theoretical research studies on an acoustic streaming[16-21] in which simple boundaries are concerned, and no studies treating such a complex vessel as that used in the present voltammetry are found. In the numerical simulation on an acoustic field and a flow field in such complex boundaries, a 2-dimensional finite element method (FEM) is considered to be the most effective method, and then the following calculations are examined. First, the sound pressure p induced by piston motion of the electrode is obtained through the numerical solution by FEM on the wave equation in Cartesian coordinates (x, y)

$$\nabla^2 p+(\omega_0/c)^2 p=0 \tag{1}$$

where ω_0 is the angular frequency of the electrode and c is the velocity of sound. Following Ref. 22), the sound pressure is calculated after the calculus of variation and the discretization on the above equation. In this case, the boundary conditions are the perfect reflective on the vessel wall and zero pressure on the free surface of the liquid. The pressure on the electrode surface which corresponds to the vibrating amplitude is derived from the acoustic impedance due to the piston motion on an infinite flat plate.[23] Here the pressures are converted to sound particle velocities u_a, v_a as

$$u_a=\frac{1}{\rho_0\omega_0}\frac{\partial p}{\partial x}, \qquad v_a=\frac{1}{\rho_0\omega_0}\frac{\partial p}{\partial y} \tag{2}$$

where ρ_0 is the density of the solution.

The acoustic forcing term to be added in the equation of motion of an incompressible viscous flow is derived from the above velocities. The equation of motion of the fluid velocity $\boldsymbol{u}(u, v)$ containing the effect of acoustic driving force $\boldsymbol{f}$ is given as

$$\frac{\partial \boldsymbol{u}}{\partial t}+(\boldsymbol{u}\cdot\nabla)\boldsymbol{u}-\nu\nabla^2\boldsymbol{u}=-\frac{\nabla p_0}{\rho_0}+\boldsymbol{f}, \tag{3}$$

where ν denotes dynamic viscosity, p_0 denotes fluid pressure, and $\boldsymbol{f}$ is shown as

$$\boldsymbol{f}=-\langle(\boldsymbol{u}_a\cdot\nabla)\boldsymbol{u}_a\rangle-\langle\boldsymbol{u}_a(\nabla\cdot\boldsymbol{u}_a)\rangle \tag{4}$$

where the brackets mean the time average.

The method of solving incompressible viscous fluid motion by 2-dimensional FEM relayed on Ref. 24). Equation (3) is transformed by employing the equation of vorticity ω defined by

$$\omega=\frac{\partial v}{\partial x}-\frac{\partial u}{\partial y}, \tag{5}$$

and the stream function denoted as ψ, to the equation of motion as

$$\frac{\partial \omega}{\partial t}+\left(\frac{\partial\psi}{\partial y}\frac{\partial\omega}{\partial x}-\frac{\partial\psi}{\partial x}\frac{\partial\omega}{\partial y}\right)-\nu\nabla^2\omega =-\frac{\partial}{\partial y}f_x+\frac{\partial}{\partial x}f_y \tag{6}$$

with

$$f_x=-\frac{\partial}{\partial x}\langle u_a^2\rangle-\frac{\partial}{\partial y}\langle u_a v_a\rangle \tag{7}$$

$$f_y=-\frac{\partial}{\partial y}\langle v_a^2\rangle-\frac{\partial}{\partial x}\langle u_a v_a\rangle. \tag{8}$$

Here we mention the additional acoustic driving force only. The righthand side of Eq. (6) is rewritten from Eqs. (7) and (8) as

$$\frac{\partial^2}{\partial x\partial y}\langle u_a^2\rangle+\frac{\partial^2}{\partial y^2}\langle u_a v_a\rangle-\frac{\partial^2}{\partial x\partial y}\langle v_a^2\rangle -\frac{\partial^2}{\partial x^2}\langle u_a v_a\rangle. \tag{9}$$

Multiplying arbitrary weighting function $\delta\omega$ and integrating over the whole region of the vessel Ω on the above expression, we take the integration by parts under the given boundary conditions. Then

$$\begin{aligned}\int_\Omega \delta\omega\left\{\frac{\partial^2}{\partial x\partial y}\langle u_a^2\rangle+\frac{\partial^2}{\partial y^2}\langle u_a v_a\rangle -\frac{\partial^2}{\partial x\partial y}\langle v_a^2\rangle-\frac{\partial^2}{\partial x^2}\langle u_a v_a\rangle\right\}d\Omega \\ =\int_\Omega\left\{\frac{\partial}{\partial y}(\delta\omega)\left(\frac{\partial}{\partial x}\langle u_a^2\rangle+\frac{\partial}{\partial y}\langle u_a v_a\rangle\right) -\frac{\partial}{\partial x}(\delta\omega)\left(\frac{\partial}{\partial y}\langle v_a^2\rangle+\frac{\partial}{\partial x}\langle u_a v_a\rangle\right)\right\}d\Omega\end{aligned} \tag{10}$$

where the integrated value over the free surface is neglected because of its smallness. Discretization on the triangle element is performed with

$$\delta\omega=\Sigma\phi_i\delta\omega_i, \qquad \phi_i=\frac{1}{2\Delta e}(a_i+b_i x+c_i y), \qquad i: 1, 2, 3.$$

ϕ_i is an interpolating function, Δe is the area of the triangle element and a_i, b_i and c_i are the function of vertical coordinates of the triangle. Then each term in Eq. (10) is given as

$$\frac{\partial}{\partial x}\langle u_a^2\rangle=\frac{\partial}{\partial x}\sum\phi_i\langle u_a^2\rangle_i$$
$$=\frac{1}{2\varDelta e}\sum b_i\langle u_a^2\rangle_i \qquad (11)$$

$$\frac{\partial}{\partial y}\langle v_a^2\rangle=\frac{\partial}{\partial y}\sum\phi_i\langle v_a^2\rangle_i$$
$$=\frac{1}{2\varDelta e}\sum c_i\langle v_a^2\rangle_i \qquad (12)$$

$$\frac{\partial}{\partial x}\langle u_a v_a\rangle=\frac{\partial}{\partial x}\sum\phi_i\langle u_a v_a\rangle_i$$
$$=\frac{1}{2\varDelta e}\sum b_i\langle u_a v_a\rangle_i \qquad (13)$$

$$\frac{\partial}{\partial y}\langle u_a v_a\rangle=\frac{\partial}{\partial y}\sum\phi_i\langle u_a v_a\rangle_i$$
$$=\frac{1}{2\varDelta e}\sum c_i\langle u_a v_a\rangle_i \qquad (14)$$

$$\frac{\partial}{\partial x}(\delta\omega)=\frac{\partial}{\partial x}\sum\phi_i\delta\omega_i$$
$$=\frac{1}{2\varDelta e}\sum b_i\delta\omega_i \qquad (15)$$

$$\frac{\partial}{\partial y}(\delta\omega)=\frac{\partial}{\partial y}\sum\phi_i\delta\omega_i$$
$$=\frac{1}{2\varDelta e}\sum c_i\delta\omega_i\,. \qquad (16)$$

Substituting above equations in the righthand side of Eq. (10), it is shown that

$$\int_\Omega\left\{\frac{1}{2\varDelta e}\sum c_i\delta\omega_i\left(\frac{1}{2\varDelta e}\sum b_i\langle u_a^2\rangle_i+\frac{1}{2\varDelta e}\sum c_i\langle u_a v_a\rangle_i\right)-\frac{1}{2\varDelta e}\sum b_i\delta\omega_i\cdot\left(\frac{1}{2\varDelta e}\sum c_i\langle v_a^2\rangle_i+\frac{1}{2\varDelta e}\sum b_i\langle u_a v_a\rangle_i\right)\right\}d\Omega$$
$$=\frac{1}{4\varDelta e^2}\left[\sum c_i\{\sum b_j\langle u_a^2\rangle_j+\sum c_j\langle u_a v_a\rangle_j\}-\sum b_i\{\sum c_j\langle v_a^2\rangle_j+\sum b_j\langle u_a v_a\rangle_j\}\right]\int_\Omega d\Omega$$
$$=\frac{1}{4\varDelta e}\left[\sum c_i\{\sum b_j\langle u_a^2\rangle_j+\sum c_j\langle u_a v_a\rangle_j\}-\sum b_i\{\sum c_j\langle v_a^2\rangle_j+\sum b_j\langle u_a v_a\rangle_j\}\right] \qquad (17)$$

j: 1, 2, 3.

The element matrix equation is constituted by adding this term to the righthand side of the equation, Eq. (5.14) in Ref. 24) for the incompressible viscous flow. Two kinds of the computational model corresponding to the equipment of the voltammetry denoted type A, and the flow visualizing vessel denoted type B are used in order to see the effects of reflected converging acoustic rays due to the circular bottom. Mesh discretizations are shown in Fig. 3(a) for type A and Fig. 3(b) for type B. The numerical constants in the calculation are as follows: the electrode vibrating frequency is 38 kHz, the velocity of sound in the solution is 1,400 m/s, and the coefficient of dynamic viscosity is 0.001 m²/s. The boundary conditions on sound field are pressure free on the surface of the solution and perfect sound reflection on the vessel wall. No shear strain is assumed in the fluid at all the region as well as no voticity at all the corners excepting the electrode edges. The values of the strength of an attached vortex pair and a detached vortex pair are assumed for the type A and type B respectively.

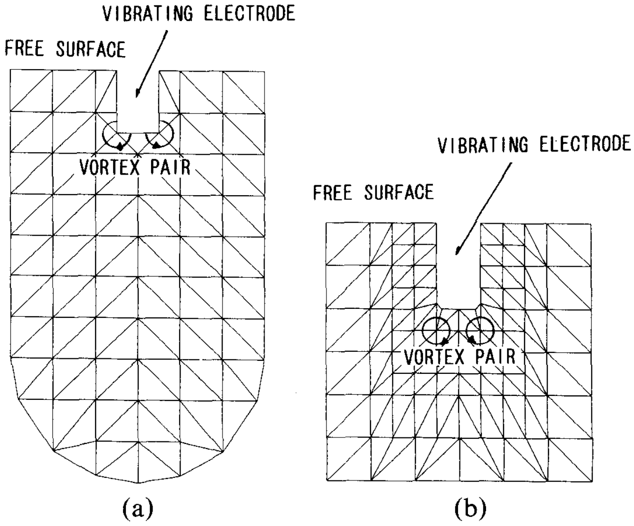

Fig. 3 (a) Mesh discretization Type A for voltammetry. (b) Mesh discretization Type B for flow visualizing vessel.

As the equation of fluid motion is time dependent, FEM time step is determined according to the condition of Courant number, to which the numerical solutions may diverge or oscillate depending on the amplitude of the electrode vibration. The decision of the convergence depends on whether the value of the mean velocity gets stationary.

The equi-sound pressure lines obtained from the solution of the wave equation are shown in Figs. 4(a) and 4(b), from which the mean sound particle velocity vectors are derived as shown in Figs. 5(a) and (b). Large outward velocity vectors are seen concentrated around the electrode. The values of velocity are substituted in the above equation of fluid motion as the driving stresses and the resulting velocity vectors at each mesh point at various sound pressures on the electrode surface are shown in Figs. 6 and 7 for the type A and B respectively. As we have concerned with the unsteady equation of fluid

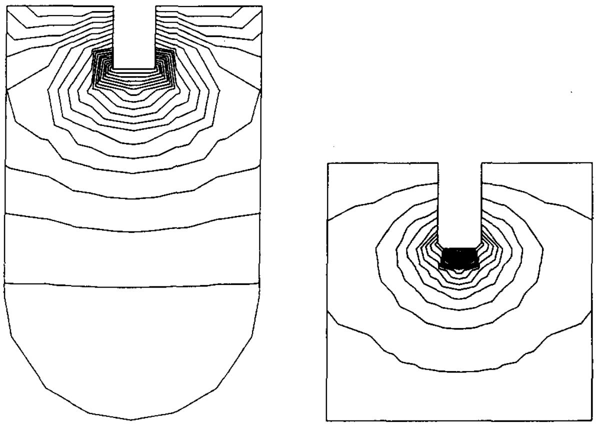

(a) (b)

Fig. 4 (a) 20 equally divided equi-sound-pressure lines in Type A at electrode pressure of 1.216×10^4 Pa. (b) Equi-sound-pressure lines in Type B at electrode pressure of 1.216×10^4 Pa.

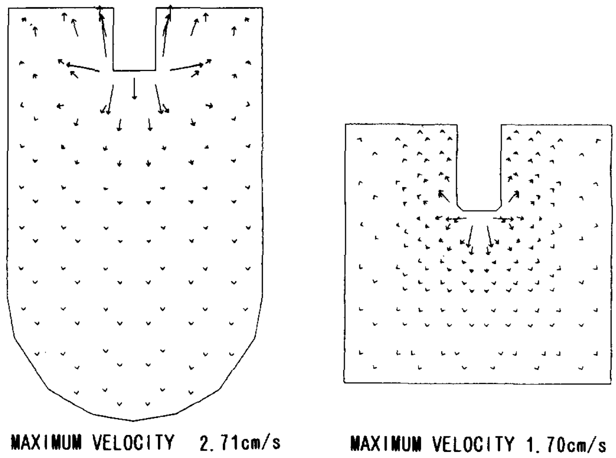

(a) (b)

Fig. 5 (a) Sound velocity vectors Type A at electrode pressure of 1.216×10^4 Pa. (b) Sound velocity vectors Type B at electrode pressure of 1.216×10^4 Pa.

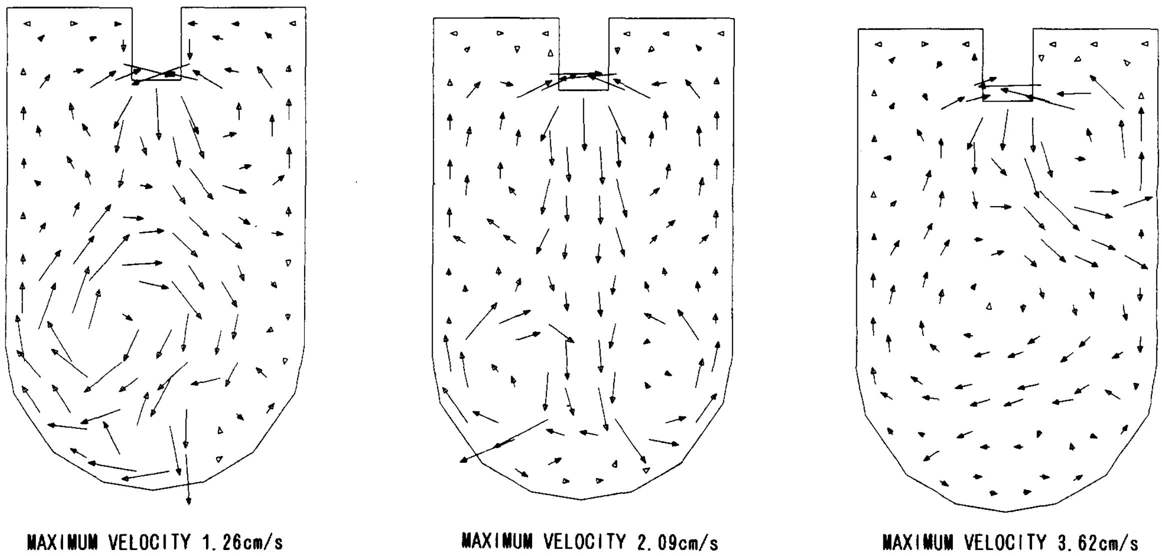

(a) (b) (c)

Fig. 6 (a) Flow velocity vectors Type A at electrode pressure of $p=1.216\times10^4$ Pa and strength of vorticity pair $\omega=\pm29.85\ \mathrm{s}^{-1}$. (b) Flow velocity vectors at $\omega=\pm59.69\ \mathrm{s}^{-1}$. (c) Flow velocity vectors at $\omega=\pm119.38\ \mathrm{s}^{-1}$.

motion, the velocity profiles change at all time but the mean velocity converges to the stationary value. The velocity profiles in these figures are not of simple laminar jets but of very complex flow, and the circulating flows emerge asymmetrically. The conjecture for the asymmetrical flow is that just like the process of the transition from laminar to turbulent flow in which a point of inflexion in the laminar velocity profile or boundary layer separation causes an unstable and asymmetrical flow. The typical example is the Kārmān vortex street behind a circular culinder. On both type A and type B, single large circulating flow is seen at a small driving sound pressure, but with the increase of the number of the circulating flow, the pressure and velocity profiles become irregular and unsteady.

As we have assumed that the vibration of the gas bubble has the same effect on a constant strength vortex pair at the electrode, then the flow with a vortex pair is confirmed to be only a simple, symmetrical and steady laminar jet flow. Both the mean and the maximum velocities for varying intensity of sound pressures at the electrode for cases with vortex pair and without vortex pair are shown in Figs. 8(a)

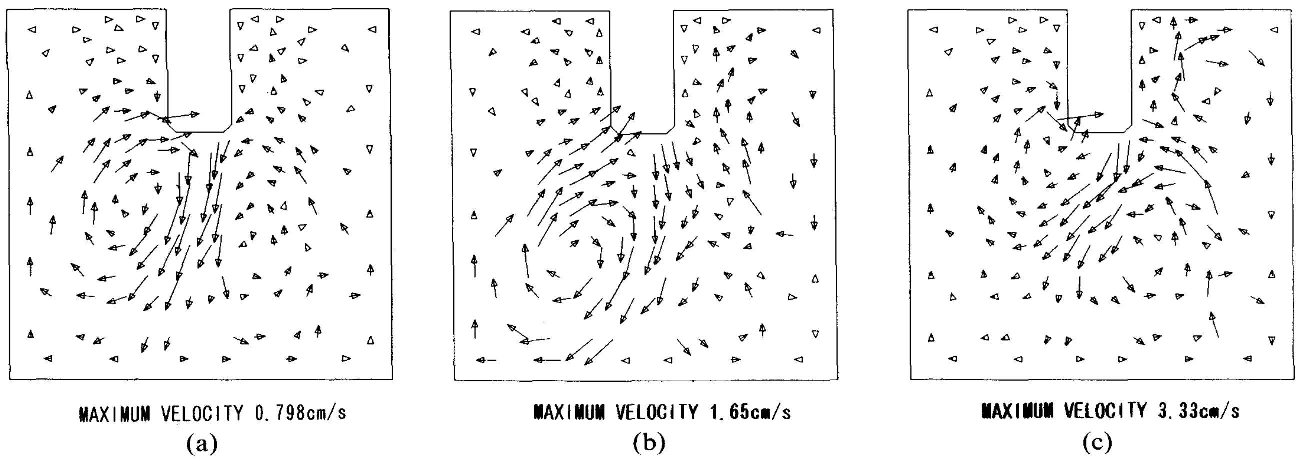

Fig. 7 (a) Flow velocity vectors Type B at vorticity pair $\omega = \pm 5.969\ \mathrm{s}^{-1}$, electrode pressure $p = 0.608 \times 10^4$ Pa. (b) Flow velocity vectors at $p = 1.216 \times 10^4$ Pa. (c) Flow velocity vectors at $p = 2.432 \times 10^4$ Pa.

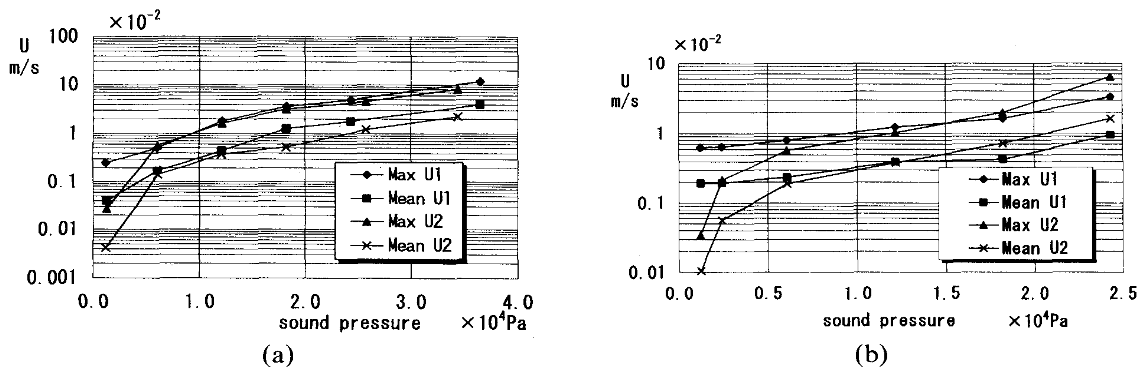

Fig. 8 (a) Maximum and mean velocity versus electrode sound pressure with strength of vortex pair $\omega = \pm 5.969\ \mathrm{s}^{-1}$, denoted by U1 and without vortex pair denoted by U2 for Type A. (b) Maximum and mean velocity versus electrode sound pressure for Type B.

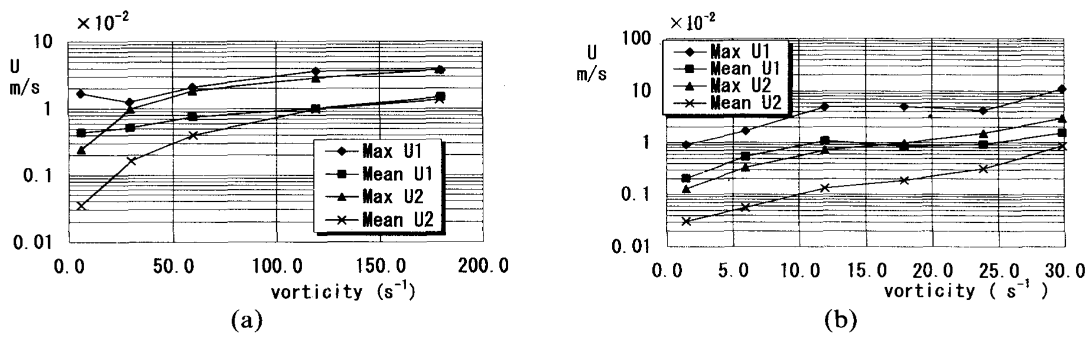

Fig. 9 (a) Maximum and mean velocity versus strength of vorticity pair with electrode pressure $p = 1.126 \times 10^4$ Pa, denote by U1 and without pressure denoted by U2 for Type A. (b) Maximum and mean velocity versus strength of vorticity for Type B.

and 8(b) respectively.

The varying vortex strength for the cases with sound drive and without sound drive is shown in Figs. 9(a) and 9(b) respectively. The maximum velocities in these figures were from 3 to 5 times larger than those of mean velocities and the effects of the vortex pair of strength $\pm 5.969\ \mathrm{s}^{-1}$ on the maximum and mean velocities were almost irrespective to the intensity of driving sound above 0.6×10^4 Pa, but the different velocity profiles were obtained. The maximum and mean velocities in the type A increase slightly with the increase of the strength of the vortex pair above $30\ \mathrm{s}^{-1}$. The same tendency is seen in the type B regarding the relation of the maximum and mean velocity to the strength of the vortex pair, but the effect of sound driving is such remarkable that the values of the maximum and mean velocities are about 8 times larger than those of the type A. The remarkable difference of velocity profiles between the type A and type B is not seen except for the larger circulating flow near the bottom of the type A vessel because the acoustic driving force is concentrated around the electrode on the present conditions.

The vibrating amplitude of 1 μm_{p-p} corresponds to the sound pressure of 1.26×10^4 Pa on the electrode surface, then the obtained maximum velocities from the visualizing experiment 1 through 3×10^{-2} m/s agree well with the simulation results. The weak sound field created by the vibrating electrode causes the flow field to be larger velocity and complex flow through the generation of the gas bubble, but as the exact relations to the mode of vibration in deformation and displacement are not clarified, it is difficult to exactly estimate the strength of the vortex pair. In practice, introducing the vortex pair, the intensity is larger than that due to the electrode edge motion, the 2-dimensional FEM simulation gives the simulated flow fields.

4. CONCLUSION

Acoustic streamings induced in the voltammetry with the ultrasonic vibrating electrode are investigated by the flow visualizing technique and numerical simulation employing 2-dimensional FEM. When the vibrating amplitude of the electrode is below 0.7 μm_{p-p}, the acoustic streamings are very weak. In the amplitudes range of 0.8 through 1.6 μm_{p-p}, a gas bubble is generated on the electrode, and stable acoustic streamings by the bubble vibration are observed. At larger amplitude range, the bubble deforms oblate and very strong acoustic streamings take place, as if the bubble shifted to another vibrating mode. In the numerical simulation by the 2-dimensional FEM, the flow field similar to that of the experiment is obtained when vortex pair is set at the electrode edge. The values of maximum and mean velocities in the simulation agreed with the observed values. The velocity profiles in the simulation are unsteady and are not exactly similar in detail with those of the experiment. Further, it is required to clarify the relations between the equivalent vortex pair strength brought about by the gas bubble vibration and the vibrating amplitude of the electrode.

ACKNOWLEDGEMENT

The authors are grateful to Professor K. Yoneda, General Education English, School of Medicine, Oita Medical University, for reviewing and improving the manuscript. Special thanks are due to Mr. H. Yoshida, Research Laboratory Center, Oita Medical University, for assistance with photography.

REFERENCES

1) B. Miller and S. Bruckenstein, "Hydrodynamic potentiometry and amperometry at ring-disk electrodes," J. Electrochem. Soc. **117**, 1032–1039 (1970).
2) B. Miller, M. I. M. Bellavance, and S. Bruckenstein, "Feasibility and applications of programmed speed control at rotating ring-disk electrodes," Anal. Chem. **44**, 1983–1992 (1972).
3) S. A. Schutte and R. L. McCreery, "Efficient hydrodynamic modulation voltammetry with a microcylinder electrode," Anal. Chem. **58**, 1778–1782 (1986).
4) S. A. Schutte and R. L. McCreery, "Hydrodynamically modulated alternating current voltammetry," Anal. Chem. **59**, 2692–2699 (1987).
5) C. M. A. Brett and A. M. O. Brett, *Electrochemistry* (Oxford University Press, Oxford, 1993), p. 151.
6) W. J. Blacedel and R. C. Engstrom, "Investigation of the ferricyanide-ferrocyanide system by pulsed rotation voltammetry," Anal. Chem. **50**, 476–479 (1978).
7) W. J. Blacedel and S. L. Boyer, "Submicromolar concentration measurements with tublar electrodes," Anal. Chem. **43**, 1538–1540 (1971).
8) R. Penn, E. Yeager, and F. Hovorka, "Effect of ultrasonic waves on concentration gradients," J. Acoust. Soc. Am. **31**, 1372–1376 (1959).
9) E. Kowalska and J. Mizera, "Influence of ultrasonic fields on processes of electric oxidation," Ultrasonics **9**, 81–84 (1971).
10) K. W. Pratt, Jr. and D. C. Johnson, "Vibrating wire electrodes-I. Literature review, design and evaluation," Electrochem. Acta **27**, 1013–1021 (1982).
11) H. D. Dewald and B. A. Peterson, "Ultrasonic hydrodynamic modulation voltammetry, Anal. Chem. **62**, 779–782 (1990).
12) M. Mohammad, "Ultrasonic voltammetry," Bull. Electrochem. **6**, 806–807 (1990).
13) W. C. Wu, A. Chiba, and K. Nakanishi, "The theoretical analysis of the jet flow on the electrodeposition of metals," Hyoumen Gijyutsu **43**, 24–29 (1992).
14) N. Tatsumoto, S. Fujii, and N. Kawano, "Ultrasonic vibrating electrode voltammetry. The electro-oxidation of chlorpromazine," Ultrason. Sonochem. **3**, 27 (1995).
15) S. A. Elder, "Cavitation microstreaming," J. Acoust.

Soc. Am. **31**, 54–64 (1959).

16) J. E. Piercy and J. Lamb, "Acoustic streaming in liquids," Proc. R. Soc. (London) **A226**, 43–50 (1954).
17) W. M. Nyborg, "Acoustic streaming," in *Physical Acoustics Principles and Methods*, W. P. Mason, Ed. (Academic Press, New York, 1965), Vol. 11, p. 265.
18) W. E. Rowe and W. L. Nyborg, "Change in an electrode process brought about small scale acoustic streaming," J. Acoust. Soc. Am. **39**, 965–971 (1966).
19) L. K. Zarembo, "Acoustic streaming," in *High Intensity Ultrasonic Fields*, L. P. Rosenberg, Ed. (Plenum Press, New York, 1971), Part III.
20) O. V. Rudenko and S. I. Soluyan, *Theoretical Foundation of Non-linear Acoustics* (Consultants Bureau, New York, 1977), p. 187.
21) H. Mitome, A. Ishikawa, H. Takeda, and K. Koyama, "Influence of attenuation of ultrasound on the driving force of acoustic streaming," IECE Tech. Rep. US 92-32 (1992) (in Japanese).
22) J. J. Conner and C. A. Brebbia (translated by T. Okumura), *Application of Finite Element Techniques for Fluid Flow Analysis* (Saiensu-sha, Tokyo, 1986), p. 135 (in Japanese).
23) P. M. Morse and K. U. Ingard, *Theoretical Acoustics* (Princeton University Press, Princeton, NJ, 1968), p. 381.
24) K. Oonishi, K. Hayashi, H. Toyama, and H. Ninomiya, "Incompressible viscous fluid," in *Flow Analysis* (Asakura Shoten, Tokyo, 1986), Chap. 5, p. 79 (in Japanese).